NASA/TM—2000-209789

Effects of G-Jitter on Interfacial Dynamics of Two Miscible Liquids: Application of MIM

Walter M.B. Duval
Glenn Research Center, Cleveland, Ohio

Bjarni V. Tryggvason
Canadian Space Agency, Saint-Hubert, Quebec, Canada

March 2000

The NASA STI Program Office . . . in Profile

Since its founding, NASA has been dedicated to the advancement of aeronautics and space science. The NASA Scientific and Technical Information (STI) Program Office plays a key part in helping NASA maintain this important role.

The NASA STI Program Office is operated by Langley Research Center, the Lead Center for NASA's scientific and technical information. The NASA STI Program Office provides access to the NASA STI Database, the largest collection of aeronautical and space science STI in the world. The Program Office is also NASA's institutional mechanism for disseminating the results of its research and development activities. These results are published by NASA in the NASA STI Report Series, which includes the following report types:

- TECHNICAL PUBLICATION. Reports of completed research or a major significant phase of research that present the results of NASA programs and include extensive data or theoretical analysis. Includes compilations of significant scientific and technical data and information deemed to be of continuing reference value. NASA's counterpart of peer-reviewed formal professional papers but has less stringent limitations on manuscript length and extent of graphic presentations.

- TECHNICAL MEMORANDUM. Scientific and technical findings that are preliminary or of specialized interest, e.g., quick release reports, working papers, and bibliographies that contain minimal annotation. Does not contain extensive analysis.

- CONTRACTOR REPORT. Scientific and technical findings by NASA-sponsored contractors and grantees.

- CONFERENCE PUBLICATION. Collected papers from scientific and technical conferences, symposia, seminars, or other meetings sponsored or cosponsored by NASA.

- SPECIAL PUBLICATION. Scientific, technical, or historical information from NASA programs, projects, and missions, often concerned with subjects having substantial public interest.

- TECHNICAL TRANSLATION. English-language translations of foreign scientific and technical material pertinent to NASA's mission.

Specialized services that complement the STI Program Office's diverse offerings include creating custom thesauri, building customized data bases, organizing and publishing research results . . . even providing videos.

For more information about the NASA STI Program Office, see the following:

- Access the NASA STI Program Home Page at ***http://www.sti.nasa.gov***

- E-mail your question via the Internet to help@sti.nasa.gov

- Fax your question to the NASA Access Help Desk at (301) 621-0134

- Telephone the NASA Access Help Desk at (301) 621-0390

- Write to:
  NASA Access Help Desk
  NASA Center for AeroSpace Information
  7121 Standard Drive
  Hanover, MD 21076

NASA/TM—2000-209789

Effects of G-Jitter on Interfacial Dynamics of Two Miscible Liquids: Application of MIM

Walter M.B. Duval
Glenn Research Center, Cleveland, Ohio

Bjarni V. Tryggvason
Canadian Space Agency, Saint-Hubert, Quebec, Canada

Prepared for the
37th Aerospace Sciences Meeting and Exhibit
sponsored by the American Institute of Aeronautics and Astronautics
Reno, Nevada, January 11–19, 1999

National Aeronautics and
Space Administration

Glenn Research Center

March 2000

Acknowledgments

We acknowledge C. Casgrain (Canadian Space Agency) and R. Bennett (NASA Glenn) for their participation in the DC-9 flight experiments that helped define the parameters for the experiments. We thank the Canadian Space Agency and NASA Glenn Research Center for their support. This experiment was flown on STS–85 in August 1997.

Available from

NASA Center for Aerospace Information
7121 Standard Drive
Hanover, MD 21076
Price Code: A03

National Technical Information Service
5285 Port Royal Road
Springfield, VA 22100
Price Code: A03

EFFECTS OF G-JITTER ON INTERFACIAL DYNAMICS OF TWO MISCIBLE LIQUIDS: APPLICATION OF MIM

Walter M.B. Duval
National Aeronautics and Space Administration
Glenn Research Center
Cleveland, Ohio 44135

Bjarni V. Tryggvason
Canadian Space Agency
CANADA, Saint-Hubert, Quebec, J3y8y9

1. Introduction

Two miscible liquids when brought into contact inside a container, in absence of any body force, will mix i.e. become homogeneous via molecular mass diffusion. Depending on the volume of liquids, spatial homogenization by random molecular motion occurs over a long time scale since the binary diffusion coefficient for liquids is on the order of $1\times10^{-5}cm^2/sec$. In the ideal situation, afforded by negligible body force, transport of mass occurs across a density interface which is relatively unaffected by large scale flows; for example stretching and folding commonly observed during mixing of cream and coffee is suppressed. Unfortunately, the presence of gravity in ground-based processing drives large scale flows which enhances mass transport. Thus the limit of mass transport via molecular diffusion, which is not affected by large scale flows, is often prohibitive in ground-based conditions.

The problem of flow fields driven by a body force is endemic to materials processing. This stems from the inherent coupling of the density field to the gradient of a thermodynamic intensive parameter (temperature and/ or concentration) driving the process. The coupling of the density field to the body force field drives buoyancy induced flow fields which can have deleterious effects on processes such as crystal growth. In addition, measurements of self and interdiffusion coefficients are severly affected by convective effects [1] . Examples of processes affected by intense convective flows are directional solidification of binary alloys, [2] physical vapor transport of acousto-optic optoelectronic materials, [3] and solution crystal growth [4,5] . Typical problems that arise are either nonhomogeneous distribution of the concentration field in the material or convective instability during processing which degrades crystalline quality.

Over the past decade, with access to a microgravity environment on the Space Shuttle, crystal growth carried out in space has shown improvement in crystalline quality as compared to their ground-based counterpart. This is attributed to the low threshold level of gravity which minimizes large scale flow fields. Thus, concentration fields are distributed uniformly and convective insta-

bilities are suppressed. However, the background gravity level on the Shuttle is not necessarily steady. Since the Shuttle behaves like a random system as it orbits the earth, its acceleration consists of a quasi-steady and a transient component due to operational activities such as orbital maneuvers, crew motion, and thruster firings for attitude control. However, there exist time intervals in which vibrations on the Shuttle are essentially quasi-steady, hence at the minimum level. These vibration levels can be approximated as a steady low background level on the order of 1 micro-g. Experiments carried out during a time interval in which the transient acceleration 'g-jitter' is intense have shown unfavorable results. In particular the solution crystal growth experiments of organic crystals [6] conducted on the Shuttle did not yield crystals with higher quality as compared to ground-based experiments. Parametric space studies on the effects of g-jitter on various processes have been carried out by a number of investigators [7,8,9,10,11,12,13] to deduce tolerable thresholds for conducting microgravity experiments.

In what follows, we describe the experimental system, present results based on well defined parametric spaces, and compare the large scale features of the interface with those predicted by a mathematical model of the system. Since the flow field was not measured during the experiment, the model complements the findings of the experiment by predicting the flow field dynamics.

Experimental System

The basic concept of the experiment is to introduce two miscible liquids positioned side by side inside a cavity, with initial vertical configuration shown in Figure 1a, and to characterize the dynamic evolution of the interface due to steady and/ or transient body force field. The subsystems necessary to carry out this experiment in a microgravity Space Shuttle environment are shown in Figure 1b. The components of the experimental system consist of a test cell, a video camera and lens, and a light source, which is mounted on the platform of the Microgravity Vibration Isolation Mount (MIM). The MIM was operated in three modes to allow the study of various body force fields on interface dynamics. These modes are the latched mode which allows transmission of g-jitter, isolation mode which isolates background g-jitter thus allowing the study of the effect of a steady body force field, and the forcing mode which allows well defined amplitude and frequency inputs as well as broadband random g-jitter type vibrations.

The test cell consists of a rectangular enclosure of height (H), width (L), and depth (W) with dimensions 5 cm, 5cm, and 1 cm respectively. The narrow width of the enclosure forces the flow field to be approximately two-dimensional. The enclosure is made from a transparent acrylic material to allow for visualization of the interface dynamics. The liquids are introduced inside the two chambers through bleeding ports at the top of the cavity using a syringe with a hypodermic needle. The enclosure consists of two sections 2.5 cm each seperated by a thin stainless steel shim (flat plate valve) of thickness 0.00375 cm. The two compartments are kept sealed by using a

thin film of vacuum grease between them, and by keeping the test cell under compression using two adjustable spring loaded clamps located at the side of the cell. The test cell is then mounted inside an acrylic enclosure and sealed for safety requirements. The vacuum grease is very effective for sealing the two compartments against leakage as well as to reduce friction when the shim is removed in order to establish the initial conditions.

The motor drive is attached to the shim which divides the two chambers. The payload motor drive consists of a 90W rated direct drive brush-type motor, limited by a linear amplifier to 30W. The motor pulls the shim from the double-chambered diffusion cell at a controlled rate. The light source is a flat backlight module, which is a sealed electroluminescent sheet lamp using 2.4W of power to generate 106 Cd/m^2 of uniform illumination.

The video camera selected for the experiment is the PULNIX-TM-7CN miniature black and white camera. The camera, 768×494 pixels, uses CCD technology to capture high quality images even at low illumination levels. The video signal is routed through the MIM to the Shuttle supplied Hi-8 video tape recorder (VTR), and from the VTR to the Shuttle-supplied laptop computer and video card for crew monitoring of the experiment.

The MIM is a system with six degrees of freedom that uses magnetic levitation to isolate a user payload from vibrational disturbances on the Space Shuttle. The MIM is composed of three modules comprising of the flotor, stator, and the front panel. The flotor is the MIM platform onto which the experimental system is mounted, it contains accelerometers to measure the effect of the control logic. The stator is underneath the flotor, the vibrations are sensed by accelerometers at the stator and countered using magnetic fields to keep the flotor suspended motionlessly. The front panel contains the control switches and connectors.

The MIM is able in principle to provide isolation at frequencies above approximately 0.02 Hz. Active control based on dual position and acceleration control loops, is used from DC to frequencies on the order of 10 Hz to 50 Hz, depending on the setting of the control parameters. Above the active control band the system provides natural mechanical isolation. In addition to being able to isolate experiments from the spacecraft vibrations, the control system can be used to input motions to the platform with well controlled acceleration levels from several micro-g to 25 milli-g in the frequency range 0.01 Hz to 50 Hz. The MIM control software can generate a very wide range of time histories for the platform motion and acceleration, tailored to the specific need of the experiment. This provides an ability to use the MIM to explore the sensitivity of experiments to g-jitter. For our experiment, we used the MIM in latched mode (transmission of the g-jitter), isolation mode, and forcing mode which isolates background g-jitter and allow the study of controlled sinusoidal forcing input to our experiment as well as single and multi-axis random vibration input. In related tests [14] the MIM demonstrated reductions in the vibration levels by two orders of magnitude.

Description of Parametric Space

Relationship between Experimental Variables and Dimensionless Parameters

We consider the effect of various types of body forces,

$$\vec{g}(t) = ng_o + mg_o\cos(\omega t + \theta), \tag{1}$$

through the use of the MIM, on the evolution of the interface between the two miscible liquids with negligible interfacial tension as shown in Figure 1a. In the above equation $\vec{g}(t)$ is a general body force field which consists of a steady and a transient component. The gravitational acceleration on Earth is denoted by g_o and n is a ratio by which this value is reduced in a Space Shuttle environment which represents the background g-level. In the second term, the ratio m denotes the amplitude, ω the frequency of the controlled acceleration from the MIM, and θ denotes its phase angle. The phase angle can be chosen to emulate a wide range of sinusoidal forcing from the MIM. Within the context of our experiment, the phase angle is an uncertainty variable. Two important limits can be considered, $mg_o \rightarrow 0$, which implies steady acceleration. In this case $n = 1$ corresponds to ground-based conditions. Whereas, n on the order of 10^{-6} indicates a steady microgravity acceleration on the Shuttle that can be obtained with the MIM operating in isolation mode. On the other hand if $ng_o \rightarrow 0$, the effect of sinusoidal forcing can be studied in detail. The range between these two limits are the cases when both terms are important. These cases serve as a framework to understand the effect of the more complex random vibration due to g-jitter. To complete our studies we also consider the effect of both single and multi-axis random vibration from the MIM for the frequency range of 0.01 - 50 Hz.

The working liquids for the experiment are selected to investigate effects of finite jump in viscosity as well as the limit of zero viscosity jump. In all cases the same composition is used for fluid B, 100% de-ionized water with a red dye (bromopyrogallol red) with a concentration of 0.005%. The nearly zero jump in viscosity liquids used for fluid A consists of dilute mixtures of de-ionized water and deuterium oxide (D_2O, 2.2% and 22%) with a methylene blue dye (0.004% concentration). Whereas the mixture with a finite jump in viscosity consists of a dilute mixture of de-ionized water and ethylene glycol (20%). The specific gravity was measured for all fluid pairs using a calibrated hydrometer (Chase Instrument), which has a range of 0.9950 to 1.0100 and a precision error to within ±0.00005. The density can be calculated from the specific gravity using ($s = \rho/\rho_w$), in which ρ_w is the density of water [15] at ambient laboratory condition. The dye concentration is kept the same for all fluid pairs. The contrast between the red and blue region facilitated tracking of the interface as it evolved with time. In this case, the interface serves as a tracer. The set of fluids with nearly zero jump in viscosity allows comparison with the single fluid model which implies continuity of velocity and shear stress at the interface,

$$\mathbf{V}^A(x,y,z,t) = \mathbf{V}^B(x,y,z,t) \quad at \quad x = L/2 \tag{2}$$

$$\sigma_{ij}{}^A(x,y,z,t) = \sigma_{ij}{}^B(x,y,z,t) \quad at \quad x = L/2 \ . \tag{3}$$

This implies that the dynamical motion of the fluid in region A and B can be described by a single momentum equation, with mean density and viscosity in the inertial and viscous terms (overbar denotes mean values). Within the context of a Boussinesq fluid, variation of the density is taken into account in the body force term,

$$\overline{\rho}\frac{D\vec{V}}{Dt} = -\nabla p + \overline{\mu}\nabla^2\vec{V} + \rho\vec{g}(t) \ . \tag{4}$$

The thermodynamic coupling of the momemtum equation to the species continuity equation is taken into account through a linear variation of density with concentration for fluid A and B, density is assumed to be independent of pressure,

$$\rho = \overline{\rho}(1 + \beta\Delta C) \ . \tag{5}$$

The coefficient of volumetric expansion due to concentration is defined as,

$$\beta = \frac{1}{\overline{\rho}}\frac{\partial\rho}{\partial C} \ . \tag{6}$$

Since we have a binary system, a single equation is necessary for the species continuity,

$$\frac{DC}{Dt} = \tilde{D}_{AB}\ \nabla^2 C. \tag{7}$$

$\tilde{D}_{AB}$ is the binary diffusion coefficient of the two liquids. The density jump discontinuity at the interface is prescribed through the initial condition,

$$t = 0 \qquad C(x,y,0) = \begin{cases} 1 & 0 \le x < L/2 \\ .5 & x = L/2 \\ 0 & L/2 < x \le L \end{cases} \ . \tag{8}$$

The concentration value of 1 and 0 corresponds to liquid A and B respectively. The interface (in particular $C = 0.5$) acts like a hypothetical material line which allows for the diffusion of mass, it behaves like a tracer which moves [16] with the mean barycentric velocity of the flow,

$$\mathbf{V} = \frac{\sum(\rho_i V_i)}{\sum\rho_i} \ . \tag{9}$$

Hence the Lagrangian history of the interface can be followed. The two fluids are incompressible, thus

$$\nabla\cdot\vec{V} = 0 \ . \tag{10}$$

Analysis shows [17] that various metrics can be used to quantify the deformation of the interface due to the body force field, the length stretch ($\tilde{L}$), interface width ($\tilde{W}$), or the concentration field (C). To discuss the effect of various parameters on the interface evolution, the most appropriate metric will be used. Scaling analysis shows that for the case in which $mg_o \to 0$, in which only the steady body force is important, the dynamics of the interface is a function of three parameters,

$$\tilde{L} = \tilde{L}(Gr, Sc, Ar) , \tag{11}$$

in which,

$$Gr=\frac{\Delta\rho n g_o}{\bar{\rho}}\frac{H^3}{\bar{\nu}^2} \quad ,(a), \qquad Sc=\frac{\bar{\nu}}{\tilde{D}_{AB}} \quad ,(b), \qquad Ar=\frac{H}{L} \quad ,(c) \tag{12a,b,c}$$

The geometry of the cavity is fixed, which implies a constant aspect ratio (Ar). The Schmidt number (Sc) can be considered as a passive variable, as its magnitude does not vary greatly. The constancy of the above parameters implies that the case for which the steady body force (ng_o) is dominant corresponds to a co-dimension one bifurcation,

$$\tilde{L} = \tilde{L}(Gr) . \tag{13}$$

The Grashof number (Gr) varies over a wide range through variation of the body force field (ng_o) from ground-based to microgravity conditions.

For the case in which both steady and transient body force are important, scaling analysis [18] shows the following parameters to be a minimum set,

$$\tilde{L} = \tilde{L}(\mathrm{Re}_s, AR, Ar) , \tag{14}$$

in which,

$$\mathrm{Re}_s=\frac{\Delta\rho}{\bar{\rho}}\frac{mg_o}{\omega^{3/2}\bar{\nu}^{1/2}} \quad ,(a), \qquad AR=\frac{\mathrm{n}}{\mathrm{m}} \quad ,(b), \qquad Ar=\frac{H}{L} \quad ,(c) . \tag{15a,b,c}$$

AR is the amplitude ratio of the steady background acceleration to the forcing amplitude from the MIM. The Stokes-Reynolds number (Re_s) represents the relative importance of buoyancy to inertia forces; it can also be written as the ratio of frequency response of the interface (ω_o) to the input frequency (ω) of the MIM,

$$\mathrm{Re}_s = (\omega_o / \omega)^{3/2} , \tag{16}$$

in which,

$$\omega_o = (\frac{\Delta\rho}{\bar{\rho}}\frac{mg_o}{\bar{\nu}^{1/2}})^{3/2} . \tag{17}$$

The amplitude ratio (AR) is also a measure of the relative importance between buoyancy flows driven by the steady to the transient component of the body force, it can be shown that

$$AR = \frac{Gr_n}{Gr_m} \quad . \tag{18}$$

The Grashof numbers based on the amplitude of the steady and transient body force are given as,

$$Gr_n = \frac{\Delta\rho}{\bar{\rho}} \frac{n g_o H^3}{\bar{\nu}^2} \quad ,(a), \qquad Gr_m = \frac{\Delta\rho}{\bar{\rho}} \frac{m g_o H^3}{\bar{\nu}^2} \quad ,(b), \tag{19a,b}$$

which shows that the amplitude ratio reduces to the ratio n/m. As mentioned earlier, since Ar is constant, the minimum set of parameters for this case corresponds to a co-dimension two bifurcation,

$$\tilde{L} = \tilde{L}(\mathrm{Re}_s, AR) \, . \tag{20}$$

Parametric Range of Experiments

The parameters of the experiments as calculated from the above dimensionless groups are shown in Table 1. Four sets of experiments (Exp. #1 -#4) were performed with the MIM in various operating modes, namely latched, isolation, and forcing. The first set of experiment (Exp #1, 2.2% D_2O) was performed with the MIM in isolation and latched mode for a total time interval of approximately 2 hours. The second set of experiment (Exp. #2, 2.2% D_2O) consisted of isolation mode used to establish the initial condition (vertical stationary interface), and various sinusoidal forcing modes with specified amplitudes (9.5 - 20 milli-g) and frequencies (.1 - 20 Hz) for a time interval of approximately 1hr and 18 minutes; the experimental cell was also excited with random forcing (0.1 - 50 Hz, 9.5 milli-g) in all three axis for approximately 83 seconds near the end of the experiment. The third set (Exp. #3, 20% ethylene glycol) was carried out for a time interval of 45 minutes, consisted of a sequence of isolation and sinusoidal forcing modes for frequencies of 10, 1, .5 Hz and corresponding amplitudes of 20, 20, 4-8 milli-g with forcing times of approximately 5 min., 4 min., 5 min. (~ 1 min. of isolation between each sequence). While in isolation mode, after the .5 Hz excitation, a primary thruster was fired (approximately 18 min. from start) which mixed the interface region. The experiment was continued, however, with a diffused interface as initial condition; the interface was excited sinusoidally (1 Hz, 20 milli-g for ~ 5 min.) and broadband random (.01 - 50 Hz, 20 milli-g for ~ 6 min.) for a single (~4 min.) and then three axes (~2 min.). The fourth set of experiments (Exp. #4, 22% D_2O) consisted of isolation initially for approximately 2 min. followed by sinusoidal forcing with various frequencies (0.1 - 1 Hz) and amplitudes (.175 - 12 milli-g) for a time interval of approximately 31 min.

For the calculation of the parameters in Table 1, the background steady acceleration ng_o on the Shuttle is approximated by $1\times10^{-6}g_o$. Note the large difference between the Grashof number for microgravity as compared to ground-based condition. For example the 2.2% D_2O sample shows a value $Gr = 3.18\times10^6$ for ground-based as compared to 3.18 in space. To demonstrate the jump in magnitude of the density needed to obtain Gr of order 1 in microgravity, we display the ratio of density jump (it can be shown that $\Delta s/\bar{s} = \Delta\rho/\bar{\rho}$). Even a low density jump of 0.0026 (2.2% D_2O) yields quite a large value of Grashof number for ground-based conditions; this reinforces the nearly ideal conditions of the dilute mixtures. Similarly, the ratio of the viscosity jump is also shown. The experiments for the steady acceleration were performed on the ground for comparison with microgravity. However, the experiments with the sinusoidal forcing mode of the MIM could not be produced on the ground, since the effect of the steady body force is overwhelming. The parameters (Re_s, n/m) for a range of frequency of interest .2 to 10 Hz are shown, the amplitudes range from 1 - 20 milli-g. The range of Re_s from 1.02×10^{-3} to 3.375×10^{-1} represents over a hundred fold in variation. For conciseness only a limited parametric range is shown in Table 1 to demonstrate order of magnitude, the remaining values are reported therein.

Mathematical Model

The experiments provide visualization of the effects the external variables have on the dynamics of the interface which essentially gives the Lagrangian history. However, since the flow field was not measured, the mathematical model fills the gap by predicting the dynamics of the flow field as well as the evolution of the interface. Thus, the model serves as a tool to understand the physics of the experiment. The prediction of the dynamics of the flow field and interface is obtained through the solution of the coupled field equations (4,7,10) consisting of the continuity, momentum, and species continuity. The boundary conditions are no slip and impermeability of the concentration field at the walls. The model is restricted to body force fields consisting of steady and transient components as shown in equation (1); the effect of broadband random force fields is beyond the scope of the present investigation. The model assumes no initial disturbance of the interface due to shim pulling. The equations are solved using finite difference techniques [19] with a flux corrected transport algorithm for interface tracking. The results of the computational model will be presented alongside the experiment.

Comparison between Ground-based and Microgravity Experiments

Microgravity Experiment

In this section we compare the results between ground-based and microgravity environments for steady acceleration and also show the effect of transmitted g-jitter. The experiment (Exp. # 1)

shown in Figure 2 was conducted for the 2.2% D_2O mixture. We will first discuss the microgravity case. The corresponding Grashof number for the microgravity condition is Gr=3.18 . For low Grashof numbers, as shown in equation 12a, the viscous force nearly balances the buoyancy force. For the time sequence shown in Figure 2(a,b,c), the MIM was operating in isolation mode. The initial configuration is shown in Figure 2a prior to the shim removal. Note the two large bubbles near the top and bottom of the cavity; in addition the vacuum grease used for sealing slightly distorts the view of the interface. After 26 sec. from removal of the shim, Figure 2b, the interface remains vertical and stationary. The slight distortion of the interface near the top of the cavity (Figure 2c, t=57 sec) is attributed to displaced fluid filling voids created by the bubbles.

The first set of results show the effectiveness of the microgravity environment to reduce buoyancy forces, hence reduction of inertial effects due to the body force field. Even though the Grashof number is not less than 1, the interface is still vertical, the other contibuting factor is the nearly two dimensionality of the experimental cell due to its small depth (1 cm) as compared to its height and width (5 cm). This result is quite remarkable given the long column of liquid, 5 cm! The implication of the interface being vertical is that the magnitude of the flow field driving mass transport between the two fluids is essentially negligible, ensuring that the two fluids will mix over a long time scale by molecular mass diffusion. In view of the field equations (4,7,10), the momentum equation is essentially decoupled from the species continuity, and the classical case of mass diffusion from a prescribed initial condition (eq. 8) can be written as,

$$\frac{\partial C}{\partial t} = \tilde{D}_{AB}\left[\frac{\partial^2 C}{\partial x^2} + \frac{\partial^2 C}{\partial y^2} + \frac{\partial^2 C}{\partial z^2}\right] \tag{21}$$

The boundary condition for the enclosure is the condition of impermeability of the concentration field normal ($\vec{n}$) to the boundary (Γ) of the wall,

$$\nabla C \cdot \vec{n} = 0 \quad \text{on} \quad \Gamma. \tag{22}$$

Since the above equation is linear, its closed form solution is,

$$C(x,y,z,t) = \left\{\frac{1}{2} + \frac{2}{\pi}\sum_{l=0}^{\infty}\frac{(-1)^l}{(2l+1)}\cos(2l+1)\pi x \cdot \exp - \left[(2l+1)^2\pi^2(\tilde{D}_{AB}/L^2)\ t\right]\right\}. \tag{23}$$

The solution implies that even for a three dimensional cavity, under the proper microgravity condition, mass transport is independent of the y and z direction and occurs in one-direction (x direction). Thus in a microgravity environment the description of mass diffusion by a one-dimensional partial differential equation, often used in the literature is actually exact! This solution is also equivalent to the common error function type solution. The concentration field as predicted by equation 23 is in agreement with the findings in Figure 2b,c in that for short times the concentration gradient at the interface is sharp as diffusion proceeds. However, over a long time scale the

concentration gradient approaches zero since the fluids become homogeneous. Even though we consider dilute systems, this experiment can be modified to allow the measurement of non-solenoidal flow [20] in a diffusion couple for non-dilute systems.

Effect of Shim Removal

Another important issue is the removal of the shim to establish the initial condition of two fluids in contact at $x = L/2$. The fact that the interface is stationary implies that fluid motion induced by viscous stress at the shim decays rapidly. Insight into this point may be obtained from the momentum equation (4), which shows that for microgravity conditions the pressure gradient which gives rise to flow is negligible since the body force is miniscule. As a result inertial effects balance viscous effects. If the cavity is approximated to be infinitely tall ($y \to \infty$), the problem reduces essentially to the classical problem of a plane boundary suddenly moved in a fluid at rest

$$\frac{\partial \mathrm{v}}{\partial t} = \bar{\nu} \frac{\partial^2 \mathrm{v}}{\partial x^2} \quad . \tag{24}$$

The coordinate system in Figure 1a may be shifted at the interface, assuming axial symmetry of the plane boundary, the boundary conditions are

$$\mathrm{v}(\mathrm{x}, 0) = 0 \ , \quad x > 0 \quad (a), \quad \mathrm{v}(0, t) = U_o \ , \quad t > 0 \quad (b). \tag{25a,b}$$

The velocity of shim removal is given by U_o. The solution [21] shows that,

$$\frac{\mathrm{v}}{U_o} = 1 - erf \ \frac{x}{\sqrt{4\bar{\nu}t}} \quad . \tag{26}$$

The denominator may be interpreted as a boundary layer thickness for which momentum diffuses,

$$\delta = 2\sqrt{\bar{\nu}t} \quad . \tag{27}$$

For our situation, when $\bar{\nu} = 0.01 cm^2/\mathrm{sec}$, t=30 sec, $x = 2.4cm$, $U_o = .2cm/sec$, $\tilde{D}_{AB} = 1\times10^{-5} cm^2/\mathrm{sec}$, the typical values are

$$\frac{\mathrm{v}}{U_o} \approx 1.8\times10^{-3} \ , \quad \delta \approx 1cm \ , \quad \mathrm{v} \approx 4\times10^{-4} cm/sec \quad .$$

The magnitude of the velocity (v) in the fluid indicates that for low pulling rates (U_o) the velocity induced by the shim removal is dissipated by viscosity quite effectively. For comparison, a characteristic velocity ($\mathrm{v}_c = \tilde{D}_{Ab}/\delta$) based on molecular mass diffusion is of order $1\times10^{-5} cm/sec$. The long time solution is not quite applicable for this situation since the time of shim removal is finite t_o (1–25*sec*). The boundary condition more appropriate to our situation is

$$\mathrm{v}(0 \ , t) = U_o \delta(t - t_o), \tag{28}$$

where δ is the impulse function for a time interval t_o. Since the velocity imparted at the boundary is not sustained for all time as implied in (25b), the disturbance velocity due to impulsive pulling of the shim would decay rather quickly. The bulk velocity of the fluids would be on the order of the characteristic velocity v_c due to transport by molecular mass diffusion. This approximate analysis shows that, for dilute systems, microgravity conditions are ideal for the single fluid model (mean density and viscosity) assumption of continuous velocity and shear stress at the interface because the initial condition of zero velocity at the interface can be approached.

Ground-based Experiment

The results of the ground-based experiment for comparison to the microgravity experiment are shown in Figure 2d-i for a Grashof number of $Gr=3.18\times10^6$. In this case the pulling velocity (U_o) was 6.78 cm/sec. Such large pulling velocity is necessary in order to allow the interface to evolve symmetrically. Due to the hydrostatic pressure imbalance, the flow field deforms the interface immediately. After 1.2 sec from the shim removal, Figure 2e shows secondary Kelvin-Helmholtz instability patterns due to the large shear stress induced by the shim. Even though care is taken to preserve symmetry of the penetration depth of the interface near the top and bottom of the cavity, slight asymmetry is observed. The bottom fluid penetrates slightly further into the cavity than the top. The flow field imparts an overturning motion which stretches and folds the interface. The complex flow field pattern induces a global heteroclinic bifurcation [22] which gives rise to an internal breakwave, Figure 2f (t=7.2 sec). The internal wave is similar to the morphology caused by Rayleigh-Taylor instability of superposed fluids. At this stage all memory from the shear induced instability caused by the shim removal is lost; the interface is smooth and continuous. The remaining sequence in Figure 2g-i shows pinching of the bubble structure (2g), collision with the wall (2h), and the decay of the oscillation from wall collision which gives rise to a diffusive mixed layer (2i). These sequence of events for a time interval of 33.1 seconds are dramatically different from the corresponding microgravity experiment for a time interval of 57 sec.

Effect of Large Initial Disturbance and Transmission of G-jitter

The effect of transmission of g-jitter (latched mode on MIM) was also investigated for the 2.2% mixture. The goal of this experiment was to investigate the effect of both isolation and latched mode, shown in Figure 2j-l, for long time intervals (total time ~ 2hrs). Unfortunately, during the shim pulling phase, a large initial disturbance was induced by the motor while the MIM was in isolation mode; a C mode was observed, Figure 2j, after approximately 7 minutes. The long time behavior of the interface is shown in Fig. 2k (1 hr.) and Fig. 2l (~ 2 hrs.). The C mode, similar to the deformation found in a rotating cylindrical liquid bridge, [23] grows and the interface becomes diffuse due to mass transport. Because of the large initial disturbance it is uncertain whether or not g-jitter transmitted by the Shuttle would cause the C mode. However, the initial disturbance initiated the C mode instability.

Comparison with Mathematical Model

The mathematical model provides insight into the physics of the experiment shown in Figure 2. To shed light on the effect of low Grashof number on the interface structure, we investigated a range of Gr from .296 to 29.6 (corresponding to Exp. #3), shown in Figure 2A. Since Gr is the important parameter, the results apply to any fluid experiment that falls in that Gr range. The results show that the interface remains stationary for all time (computation shown for 1 hr) only when Gr < 1. The flow field is of the order of the mass diffusion velocity scale ($V = 4.97\times10^{-6} cm/sec$). Though there is fluid motion, as shown by the streamfunction and vector field plots, however the interface is not deformed (Gr=.296 case). This result compares well with the prediction of the concentration field given by equation (23). However, for Gr=29.6, the interface deforms into an S shape, similar to a two mode symmetric pattern. Thus one should be careful in interpreting two mode instabilities due to vibration, since it can also be caused by a steady background acceleration.

Comparison of the cases in Figure 2 with mathematical predictions is shown in Figure 2B. Note that the microgravity case (Figure 2B,a-c) shows excellent agreement with experiment. Even though Gr= 3.18, for short time intervals the interface does not deform as shown in Figure 2A. The streching and folding of the interface is captured for the ground-based condition ($Gr=3.18\times10^{6}$, Figure 2B,e-g), as well as the wall collision event and the stable stratification (Figure 2B,h-i). Though the conditions necessary to predict the C mode are beyond the scope of the model (random vibration), it was found that reversing the orientation of the steady acceleration (Figure 2B,j-l) causes the bottom half of the interface to deform in the same direction as the C mode.

Effect of Sinusoidal Forcing Input from MIM

Exp.#2, 2.2% D_2O

The effect of sinusoidal forcing for Exp.# 2 (2.2% D_2O) and Exp. #3 (20% Eth.) is shown in Figure 3. The response of the interface is determined by the magnitude of the Stokes-Reynolds number Re_s; as shown in Table 1 for Exp. #2, Re_s ranges from 1.02×10^{-3} to 1.83×10^{-1} for the frequency band of .2 to 10 Hz. The response to sinusoidal excitation is shown in Figure 3a,b, which indicates that for Re_s on the order of .183 the interface bifurcates to a low amplitude 3 mode quasi-stationary wave oriented vertically. With continuous forcing and a broadband random excitation in three axes (0.1 - 50 Hz, 9.5 milli-g) near the end of the experiment, the amplitude of the wave increases slightly and a band of diffusive layer (Figure 3c) is clearly visible after ~ 1 hour indicating local mass transport.

Exp.#3, 20% Ethylene Glycol

The sequence of events for Exp. #3 (20% Eth.) is shown in Figure 3d-l. In Figure 3d, after removal of the shim during isolation (t= 11 sec), the interface is clearly stationary and vertical. The interface remains stable against excitation with 10 Hz and 20 milli-g ($Re_s = 1.06\times10^{-2}$, Figure 3e-f), however the striation thickness increases. The interface becomes unstable against Kelvin-Helmholtz instability, due to parallel shear generated by the flow field for the 1 Hz (Re_s=.3375) sequence, Figure 3g-i. After 238 seconds of excitation, Fig. 3i, a four mode quasi-stationary wave evolves. The quasi-stationary wave is slightly asymmetric along its axis; with respect to the bottom of the cavity the wavelength decreases slightly whereas the amplitude increases. The wave was subsequently injected with energy which contained a range of amplitude (4-8 milli-g) while keeping the frequency constant at 0.5 Hz. This action caused an increase in amplitude of the quasi-stationary wave, Fig. 3j-l.

Mathematical Prediction of Effect of Sinusoidal Forcing

During sinusoidal forcing, there exists a mean steady background acceleration, we show the interplay between the effect of the steady and transient acceleration in Figure 3A. This figure demonstrates that the mean flow can destabilize the parallel shear flow ($ng_o=10^{-8}g_o$, Figure 3A-a) and cause a rotational flow ($ng_o=10^{-6}g_o$, Figure 3A-c) which deforms the interface. Unlike the regions in which the steady or transient component of the body force dominates, in the transition region, ($ng_o=10^{-7}g_o$, Figure 3A-b) both the parallel shear and rotational components of the flow interact. The parallel shear flow, Fig. 3A-a, is an example of a typical flow field which can generate Kelvin-Helmholtz instability to produce quasi-stationary waves. This example demonstrates that high frequency excitations (10 Hz or greater) are not effective in causing the interface to become unstable, while the mean steady acceleration can be more effective in that regard.

Comparison between the experimental results in Figure 3 and its computational prediction is shown in Figure 3B. The low amplitude response superimposed on the diffusive interface for Exp. #2 (Figure 3B,a-c) is predicted quite well with sinusoidal forcing. For Exp. #3, the interface remains stable against 10 Hz excitation (Figure 3B,d-f) however there is some diffusion which increases the striation thickness, in agreement with the experiment. The four mode quasi-stationary wave due to Kelvin-Helmholtz instability is also predicted reasonably well for the 1 Hz (Figure 3B,g-i) and .5 Hz (Figure 3B,j-l) excitation, however, subtle differences exist on the angle of the contact line with respect to the wall and symmmetry. The angle of the contact line near the wall is predicted to form a vertical tangent whereas the experiment shows the contact line has a horizontal tangent. Such a deviation is possibly attributed to effects of phase angle.

Effect of Primary Thruster Fire and Excitation of Diffusive Interface

The effect of primary thruster fire and excitation of a diffusive interface is shown in Figure 4 (Exp. #3, 20% Eth.). During the isolation mode, after the 0.5 Hz excitation, the primary thruster was fired (Figure 4a-c); a catastrophic bifurcation occured which resulted in incipient mixing of the interface. It appears that the long wavelength instability (Fig. 4a) cascaded to shorter and shorter wavelengths (Fig. 4b-c) similar to a turbulent cascade. The thruster fire which is a large amplitude random vibration input to the system lasted for ~ 5 sec. Subsequently the interface was excited with .1 Hz and .15 milli-g (Fig. 4d-f), since Re_s is miniscule, the interface remains stable against the purturbation. The tilt shown in Fig. 4d is due to momentum imparted to the flow field from residual effects after the thruster fire; the interface subsequently stabilized (Fig. 4f).

The diffusive interface was subsequently excited (Fig. 4g-i) sinusoidally with the same frequency and amplitude as shown in Fig. 3B,g-i which resulted in the four mode quasi-stationary wave. The response of the interface after 48 sec. of excitation (Fig. 4g) shows a symmetric two mode response. In contrast to the excitation of a sharp interface, the reduction of the number of modes is likely due to dissipation of the input energy by the diffusive interface. For increased excitation time the symmetric two mode bifurcates to a Z mode (Fig. 4i). The length of the interface stretches while its striation thickness decreases, a clear indication of mass transport. The effect of single and multi-axis broadband random excitation (0.01-50 Hz, 20 milli-g) is shown in Figure 4j-l. The single axis random forcing (Fig. 4j,k) does not produce significant change in the Z profile, except for the angle of the contact line at the top and bottom boundary which forms a vertical tangent (90^o contact angle). With three-axes random excitation (Fig. 4l) the interface slightly thickens due to mass transport, the vertical tangent of the contact lines at the top and bottom boundaries becomes more pronounced.

Model Prediction of Sinusoidal Excitation of Diffusive Interface

The effect of reduction of mode numbers observed in the experiment for sinusoidal excitation of a diffusive interface corresponding to Figure 4f-i was investigated. Figure 4A shows the response of a diffusive interface (Fig. 4A-a) to a single and multi-axis (Fig. 4A,e-j) excitation; the phase angle θ was varied as well. It was found that the phase angle determines the direction of tilt of the interface. In agreement with the experiment, the excitation (1 Hz, 20 milli-g) of the diffusive interface (Figure 4A-a) results in a decreasing number of modes. The interface bifurcated to a symmetric two-mode quasi-stationary wave (Fig. 4A,b-d) similar to the experiment, however, the Z mode did not evolve. The Z mode was found to occur for multi-axis excitation with various phase angles. Fig. 4A,e-f shows the genesis of the Z mode in which part of the interface is stretched for a phase angle of 90^o. Results for a phase angle of 180^o (Fig. 4A,h-j) show the same interface orientation as the experiment, however for a phase angle of 10^o the interface tilts in the reverse direction.

Sinusoidal Forcing Input from MIM for Exp. #4

The effect of sinusoidal forcing for Exp. #4 (22% D_2O) is shown in Figure 5. The parametric range for this case bridges the gap between Exp. # 2 and Exp. #3. During the isolation mode, after the shim is removed (t=5 sec), the interface remains vertical (Fig. 5a); however, after 130 sec of isolation the interface deforms to an asymmetric S profile. The S profile is attributed to the effect of the buoyancy force, since the Grashof number (Gr=26.9) is substantially larger as compared to Exp. #1 (Gr=3.18). In addition the viscosity jump for this system is nearly zero as compared to Exp. #3, there is less resistance to perturbations. Excitation of the interface (Fig. 5c) with .5 Hz and 2.5 milli-g (Re_s=.097) does not cause appreciable change from the isolation mode (Fig. 5b); the mean field most likely dominated the oscillatory component. Subsequent excitation with 1 Hz, 8 milli-g (Re_s=.109, Fig. 5d-f) did not cause any noticeable change in the deformation of the interface. The computational model indicates that the deformation is due to the steady component of the body force; it is overwhelming in comparison to the transient. However, with excitation of 0.1 Hz and amplitude range from 0.175 - 0.2 milli-g (Fig. 5g-i, $Re_s \approx 2.4\times10^{-3}$), the interface responds with a two mode symmetric bifurcation in agreement with the computational findings. In this case the effect of the transient component of the body force dominated the steady component.

Model Prediction for Exp. #4

The model prediction of Exp. #4 are shown in Figure 5A. The stationarity of the interface for short time (Figure 5A-a) agrees with the experiment, however, the penetration depth of the S profile (Fig. 5A-b) was less than that found in the experiment. Excitation with .5 Hz (Fig. 5A-c) did not substantially affect the interface. It was found that for the 1 Hz excitation the S profile is due to the steady component of the body force rather than the transient (Fig. 5A,d-f), however, the asymmetry was not predicted. The two mode quasi-stationary wave was found to occur for the .1 Hz excitation (Fig. 5A,g-i) with some difference in the angle of the contact line near the boundaries. Overall, the model predicted the large scale features of the experiment and shed light on the flow field dynamics. Issues on asymmetry and contact line angle at the boundary remains to be resolved.

Summary and Conclusions

We performed a flight experiment to study effects of sinusoidal and g-jitter type of body force on the dynamics of a vertical density interface between two miscible liquids using the MIM. With the MIM in isolation mode, the interface between the two fluids remain vertical for low Grashof numbers. This finding proves that microgravity is ideal for achieving conditions in which transport is dominated by molecular mass diffusion. Studies on the effect of long term isolation and latched mode (transmission of g-jitter) was inconclusive due to a large disturbance caused by the motor during shim removal, however, the interface bifurcated to a C mode.

Excitation of the interface with sinusoidal frequencies in the range of .1 to 10Hz and amplitudes of 0.2 to 20 milli-g show regions of stability as well as bifurcation to two, three, and four mode quasi-stationary waves. The quasi-stationary waves are caused by Kelvin-Helmholtz instability due to a parallel shear flow at the interface and shown to correlate with the Stokes-Reynolds number (Re_s); the four mode quasi-stationary wave occurs at Re_s=.3375. Effect of primary thruster fire was captured and caused a catastrophic bifurcation which mixed the interface region. Excitation of a diffusive interface with sinusoidal forcing results in a decrease of mode numbers; the two mode symmetric quasi-stationary wave bifurcated to a Z mode. The effect of broadband random excitation enhanced stretching of the Z mode, which increases mass transport. The mathematical model predicted the overall features of the experiment quite well, however issues of asymmetry and angle of the contact line with the wall need further investigation. These experiments show that the MIM is effective to isolate against vibrations that cause convection in non-homogeneous fluids, otherwise transport by molecular mass diffusion cannot be readily achieved. Given the high probability of vibration driven convection without isolation, the potential effects of g-jitter should be considered for experiments planned for the International Space Station.

Acknowledgement

We acknowledge C. Casgrain (Canadian Space Agency) and R. Bennett (NASA Glenn) for their participation in the DC-9 flight experiments that helped define the parameters for the experiments. We thank the Canadian Space Agency and NASA Glenn Research Center for their support. This experiment was flown on STS-85 in August 1997.

References

1) Frohberg, G., Kraatz, K. H., and Wever, H., 1987, *Diffusion and transport phenomena in liquids under microgravity.* Proc. 6th European Symposium on Materials Science Under Microgravity Conditions, Bordeaux, France, (ESA SP-256) 585-591, 2-5 December 1986.

2) Alexander, J.I.D., Amiroudine, S., Ouazzani, J., Rosenberger, F., *Analysis of the low gravity tolerance of Bridgman-Stockbarger crystal growth, II. Transient and periodic accelerations.* J. Crystal Growth, Vol. 113, pp 21-38, 1991.

3) Duval, W.M.B., Singh, N.B., Glicksman, M.E., *Physical vapor transport of mercurous chloride crystals: Design of a microgravity experiment.* J. Crystal Growth, 174, pp. 120-129, 1997.

4) Galster, G., and Nielsen, K. F., *Crystal growth from solution.* Proceedings of the 5th European Symposium on Materials Sciences under Microgravity, Schloss Elman, W. Germany, pp. 189-191, 1984.

5) Gerbi, D.J., Egber, W.C., Ender, D.A., Leung, P.C.W., Rochford,K.B., Virden, J.W., Cook, E.L., *Growth of organic crystals in a microgravity environment.* Journal of Crystal Growth, Vol. 76, 673-680, 1986.

6) Radcliffe, M. D., Steffer, J. E., Cook, E. L., Cotting, J. F., Miller, C. R., Drake, M. C., Schroeder, F. S., and Stevens, Jr., D., *Organic crystals in low earth orbit,* J. of Crys. Growth, Vol. 92, 581-590, 1988.

7) Farooq, A., Homsy, G.M., *Streaming flows due to g-jitter induced natural convection.* J. Fluid Mech., Vol. 271, p. 351, 1994.

8) Monti, R., Langbein, D., Favier, J.J., *Influence of residual accelerations on fluid physics and materials science experiments.* in Fluids Sciences and Material Sciences in Space: A European Perspective, edited by H.U. Walter, Springer-Verlag, Berlin, p 637-680, 1987.

9) Alexander, J.I.D., *Low gravity experiment sensitivity to residual acceleration: A review.* Microgravity Science and Technology, Vol 3, p. 52, 1990.

10) Alexander, J.I.D., Amiroudine, S., Ouazzani, J., Rosenberger, F., *Analysis of the low gravity tolerance of Bridgman-Stockbarger crystal growth,II. Transient and periodic accelerations.* J. Crystal Growth, Vol. 113, pp 21-38, 1991.

11) Zhang, W., Casademundt, J., Vinals, J., *Study of the parametric oscillator driven by narrow band noise to model the response of a fluid surface to time-dependent accelerations.* Phys. Fluids A, Vol 5, p. 3147, 1993.

12) Casademundt, J., Zhang, W., Vinals, J., Sekerka, R.F., *Narrow band noise as a model of time-dependent accelerations: study of the stability of a fluid surface in a microgravity environment.* Proc. 31st Aerospace Sciences Meeting, Paper AIAA-93-0910, Jan. 1993.

13) Kamatoni, Y., Prasad, A., and Ostrach, S., *Thermal convection in the enclosure due to vibrations aboard spacecraft.* AIAA Journal, Vol. 19, No. 4, pp 511-516, 1981.

14) Tryggvason, B.V., and Hails, E., *The microgravity vibration isolation mount (MIM), summary of MIM operations on mission STS-85, August 7-19, 1997.* Canadian Space Agency Report CSA-CAP.197, July 31, 1998.

15) Lide, D.R., Frederikse, H.P.R., *CRC Handbook of Chemistry and Physics,* 77th ed., CRC Press Inc., pp. 6-9 - 6-10, 1996-1997.

16) Perera, P.S., Sekerka, R.F., *Nonsolenoidal flow in a liquid diffusion couple.* Physics of Fluids, Vol. 9 No. 2, pp. 376-391, 1997.

17) Ottino, J. M., *Description of mixing with diffusion and reaction in terms of the concept of material surfaces,* J. Fluid Mech., 114, 83-103, 1982.

18) Duval, W.M.B., *Numerical study of mixing of two fluids under low gravity.* NASA TM 105865, 1992.

19) Duval, W.M.B., *The kinematics of buoyancy induced mixing,* Proceedings of the VIIIth European Symposium on Materials and Fluid Sciences in Microgravity, Universite Libre de Bruxelles, Belgium, April 12-16, pp 855-861, 1992.

20) Duval, W.M.B., and Jacqmin, D.A., *Interfacial dynamics of two liquids under an oscillating gravitational field.* AIAA Journal, Vol. 11, No. 11, pp 1933-1941, 1990.

21) Batchelor, G.K., *An Introduction to Fluid Dynamics.* Cambridge Unibersity Press, 1967.

22) Duval, W.M.B., *Flow field topology of buoyancy induced mixing.* Proc. of the 34th Aerospace Sciences Meeting & Exhibit, AIAA-96-0253, 1996.

23) Da Rivera, I. and Martinez, I., Proc. 3rd Europ. Symp. Mats. Sci. Space, ESA SP-142, 67, 1979.

TABLE 1.—PARTIAL EXPERIMENTAL MATRIX, $ng_o \sim 10^{-6}\ g_o$

Sample	Gr_e (Ground-based)	Gr_s (Microgravity)	f(Hz)	m	Res	$\frac{\Delta\rho}{\bar{\rho}}$	$\frac{\Delta\nu}{\bar{\nu}}$	n/m
Exp. #1 and #2 2.2%D_2O+H_2O	3.18×10^{6}	3.18	10	2×10^{-2}	1.02×10^{-3}	0.0026	~0	5×10^{-5}
Exp. #2 2.2%D_2O+H_2O	------	3.18	1	2×10^{-2}	3.24×10^{-2}	0.0026	~0	5×10^{-5}
Exp. #2 2.2%D_2O+H_2O	------	3.18	0.2	1×10^{-3}	1.83×10^{-1}	0.0026	~0	1×10^{-3}
Exp. #3 20% Eth.+H_2O	2.96×10^{7}	29.6	10	2×10^{-2}	1.06×10^{-2}	0.028	0.146	5×10^{-5}
Exp. #3 20% Eth.+H_2O	------	29.6	1	2×10^{-2}	3.375×10^{-1}	0.028	0.146	5×10^{-5}
Exp. #3 20% Eth.+H_2O	------	29.6	0.5	8×10^{-3}	3.818×10^{-1}	0.028	0.146	1.25×10^{-4}
Exp. #4 22%D_2O+H_2O	2.69×10^{7}	26.9	1	2×10^{-2}	2.734×10^{-1}	0.022	~0	5×10^{-5}
Exp. #4 22%D_2O+H_2O	------	26.9	0.5	8×10^{-3}	3.094×10^{-1}	0.022	~0	1.3×10^{-4}
Exp. #4 22%D_2O+H_2O	------	26.9	0.2	1×10^{-3}	1.529×10^{-1}	0.022	~0	1×10^{-3}

Eth. ≡ Ethylene glycol

Cell dimensions = 5×5×1 cm

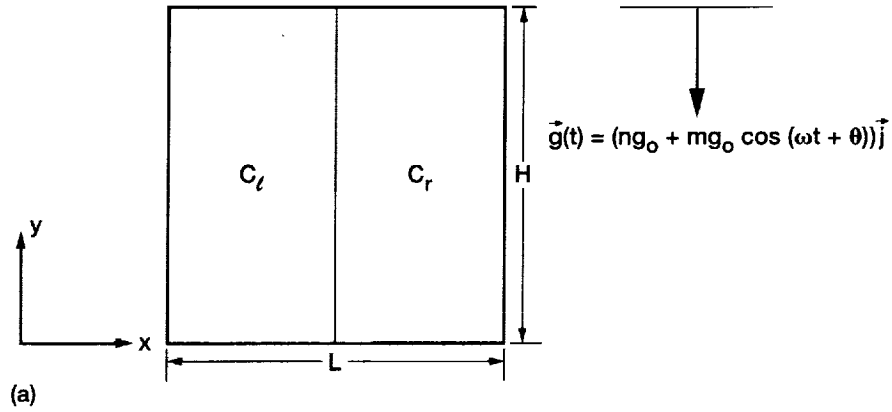

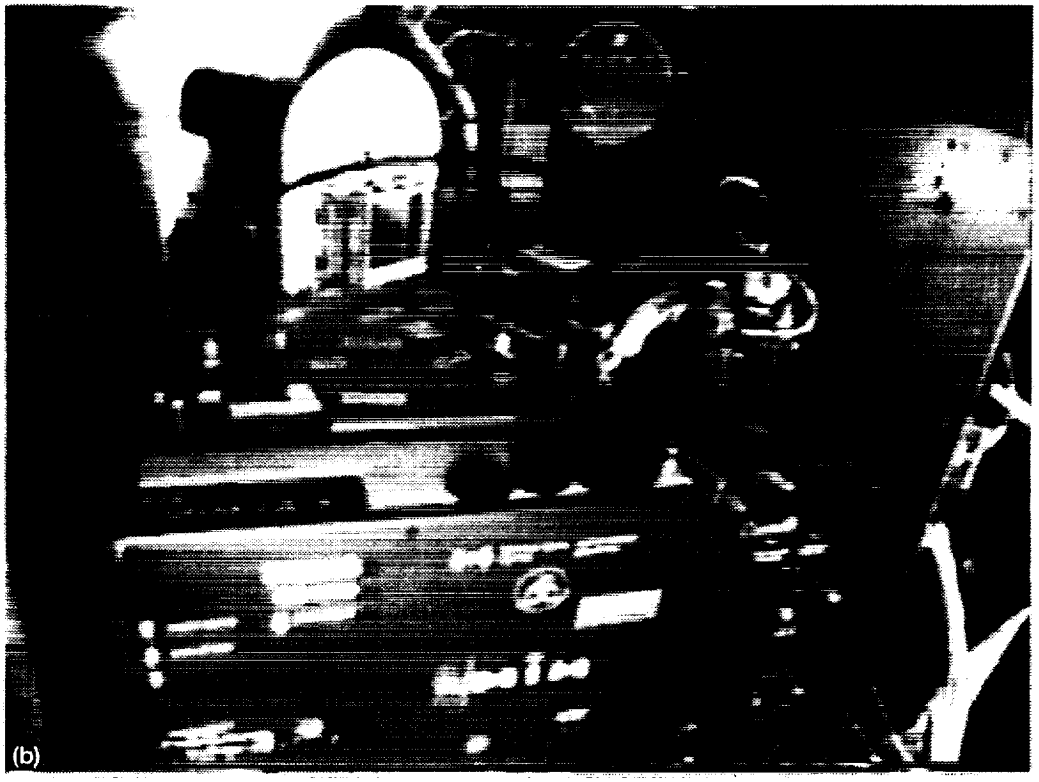

Figure 1.—(a) Physical description of two fluids in contact at an interface. (b) Experiment mounted on the Microgravity Vibration Isolation Mount (MIM) platform on STS-85.

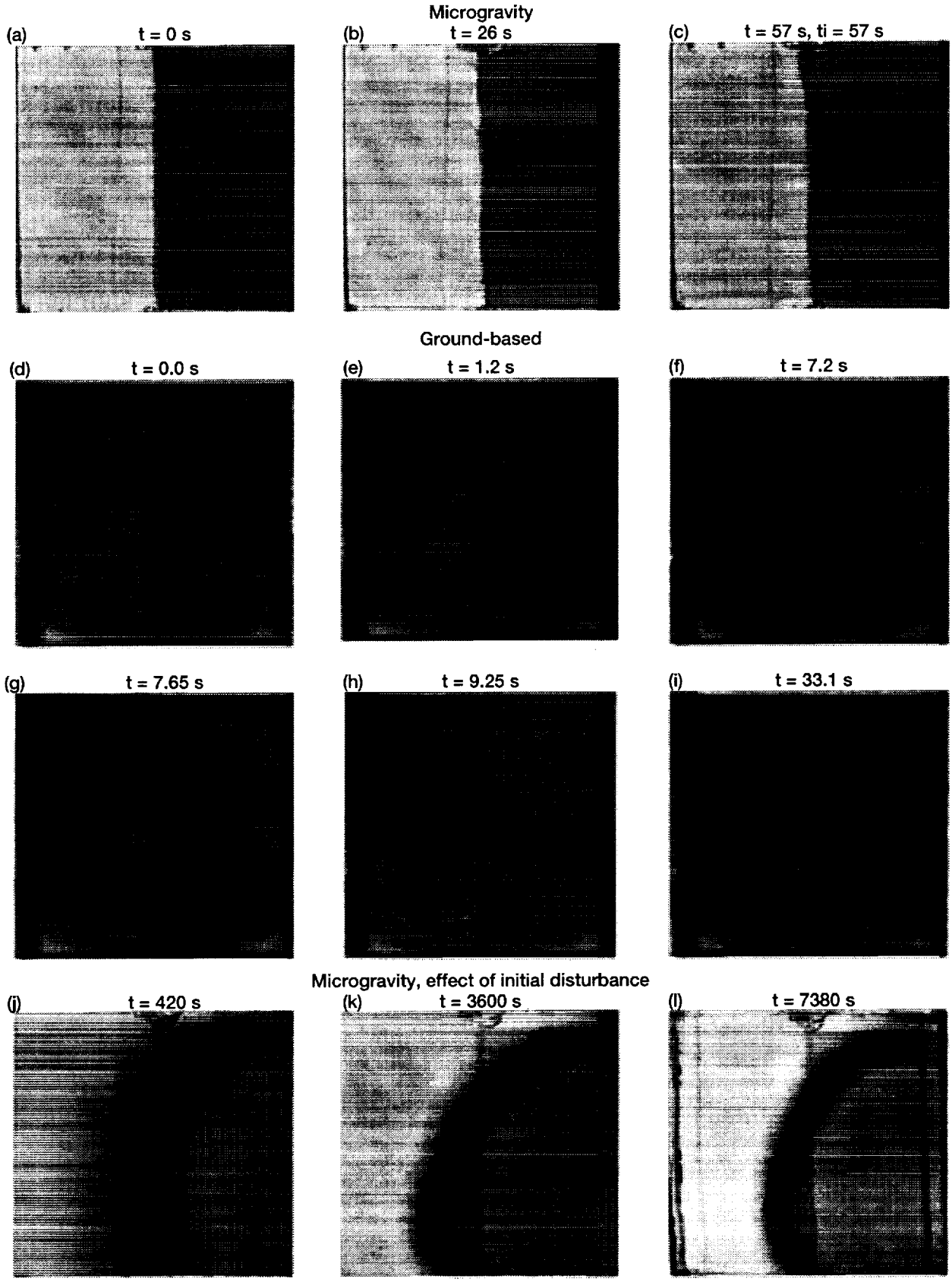

Figure 2.—Steady acceleration results contrasting microgravity and ground-based environment, (t - time relative to shim removal, ti - isolation time).

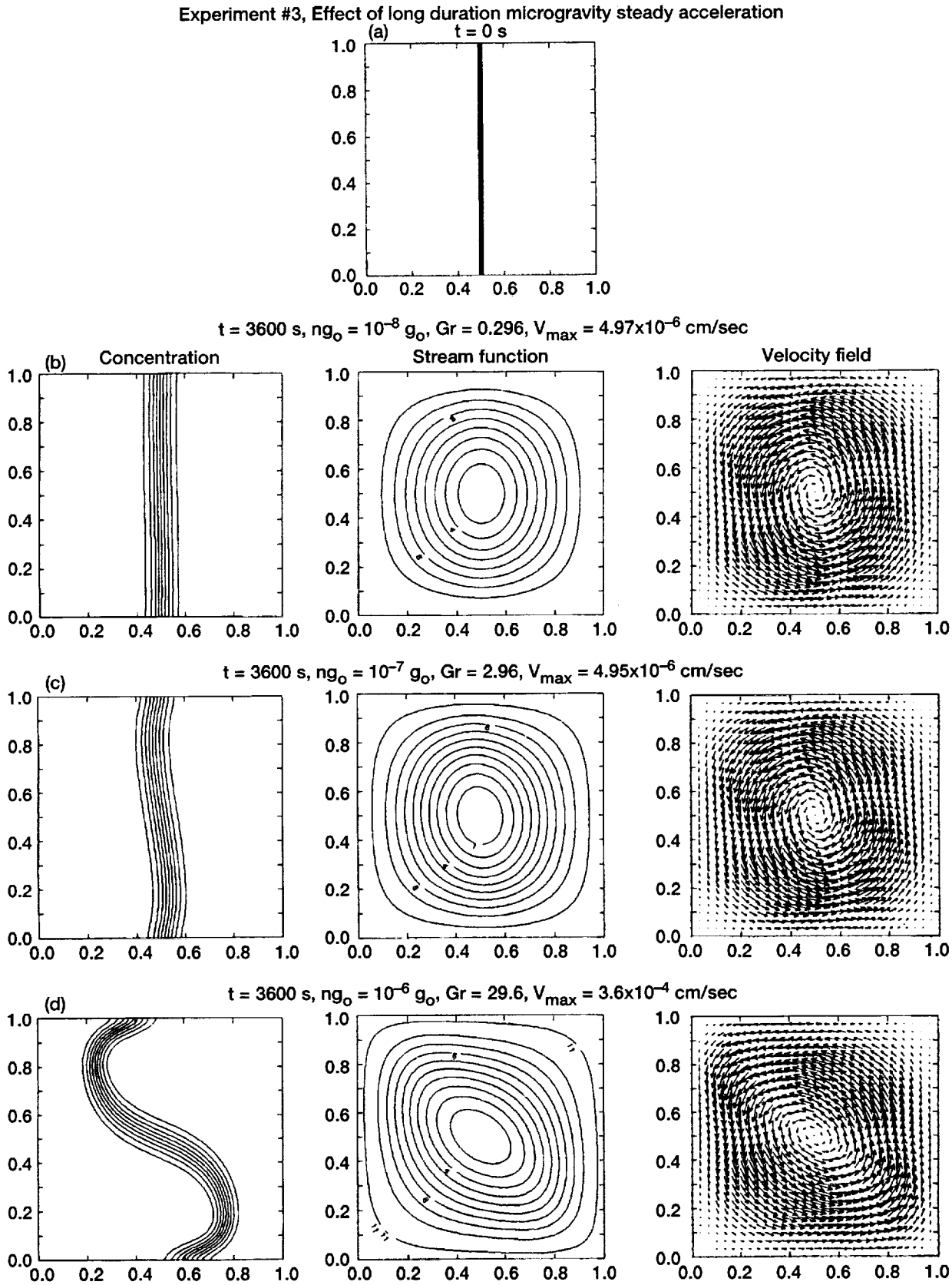

Figure 2A.—Deformation of the interface due to increase in intensity of the flow field induced by increasing the threshold of the steady acceleration.

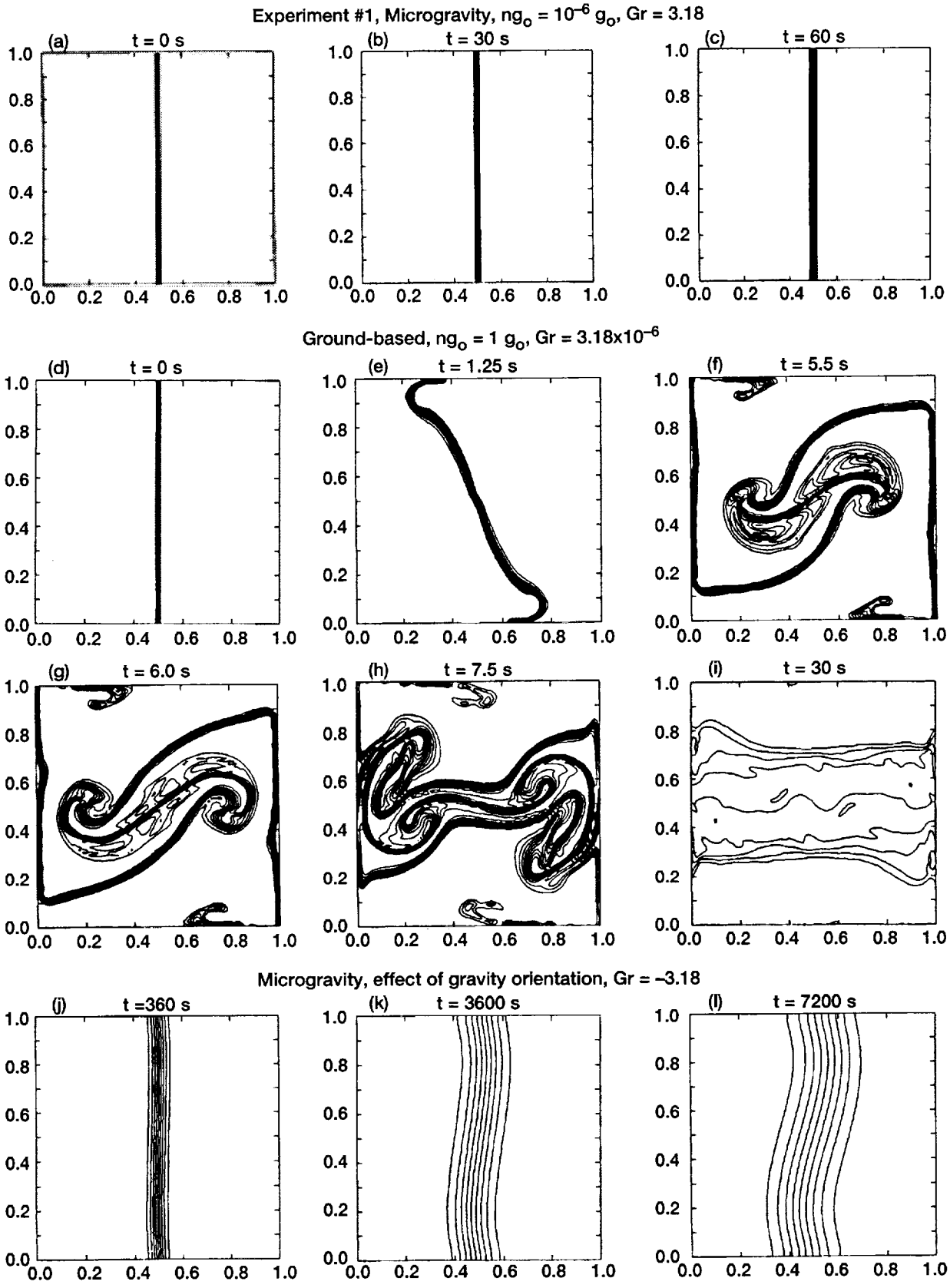

Figure 2B.—Comparison of microgravity and ground-based conditions as predicted with mathematical model for steady acceleration.

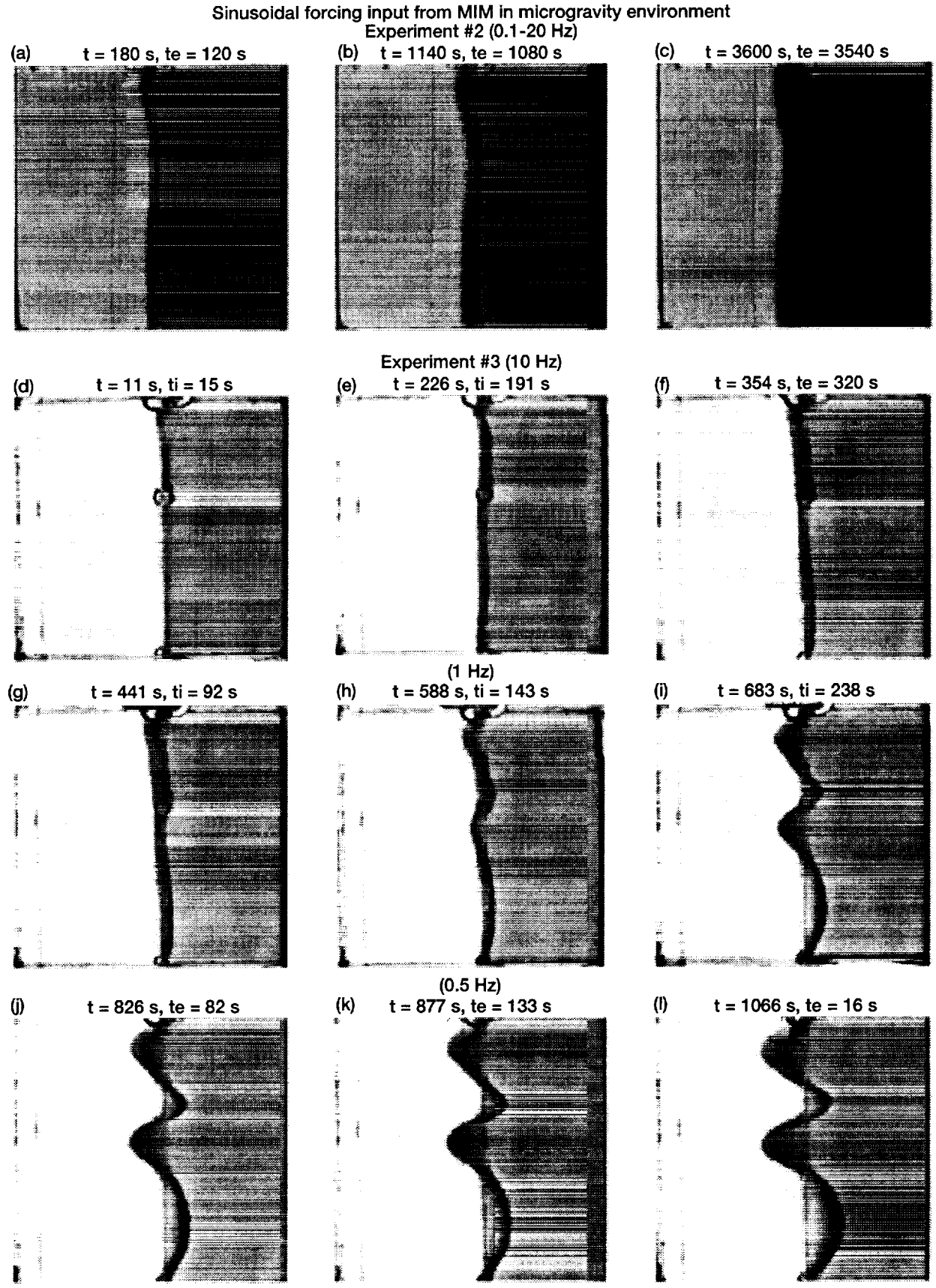

Figure 3.—Evolution of the interface due to various sinusoidal and random (exp. # 2c) forcing input from the MIM, (t - time relative to shim removal, ti - isolation time, te - excitation time).

Experiment #3, Interplay between high frequency excitation and rotational flow

(a) t = 800 s, $ng_o = 10^{-8}\ g_o$, f = 10 Hz, mg_o = 20 mg, Re_s = 0.0107, $V_{max} = 4.77 \times 10^{-4}$ cm/sec

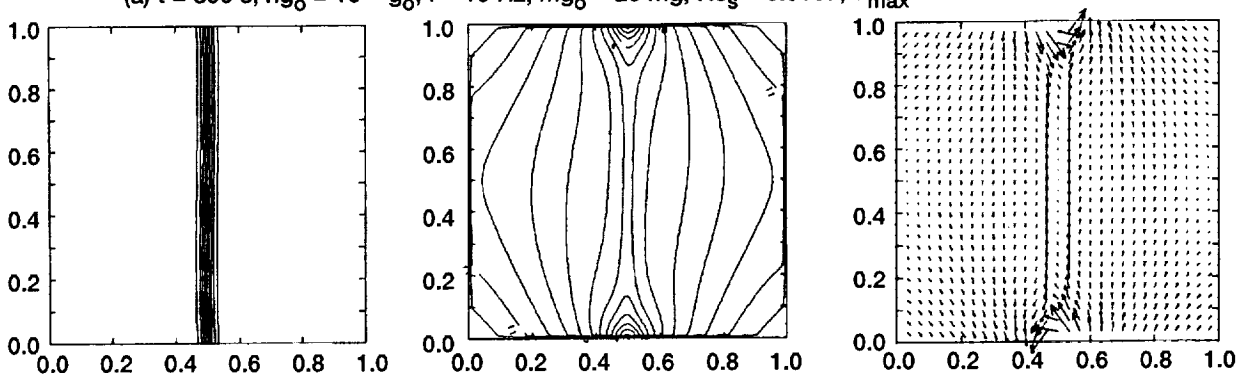

(b) t = 800 s, $ng_o = 10^{-7}\ g_o$, f = 10 Hz, mg_o = 20 mg, Re_s = 0.0107, $V_{max} = 4.85 \times 10^{-4}$ cm/sec

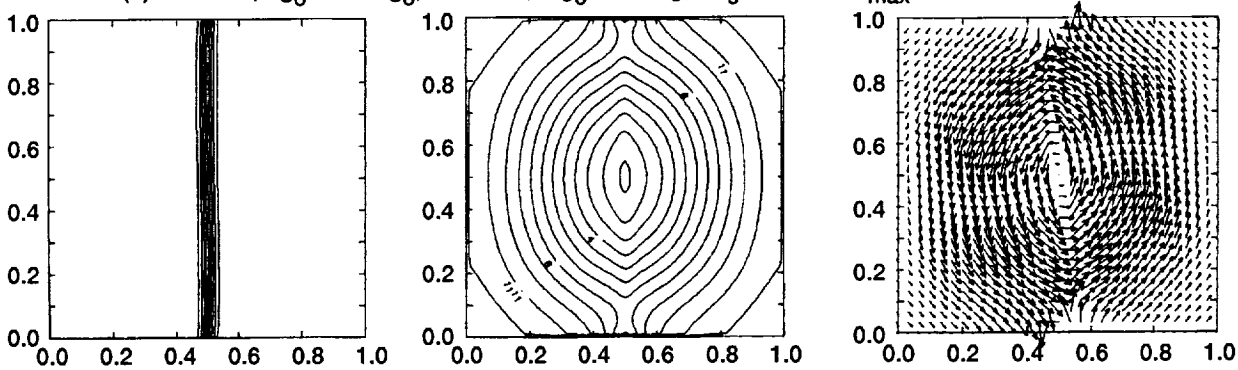

(c) t = 800 s, $ng_o = 10^{-6}\ g_o$, f = 10 Hz, mg_o = 20 mg, Re_s = 0.0107, $V_{max} = 5.4 \times 10^{-4}$ cm/sec

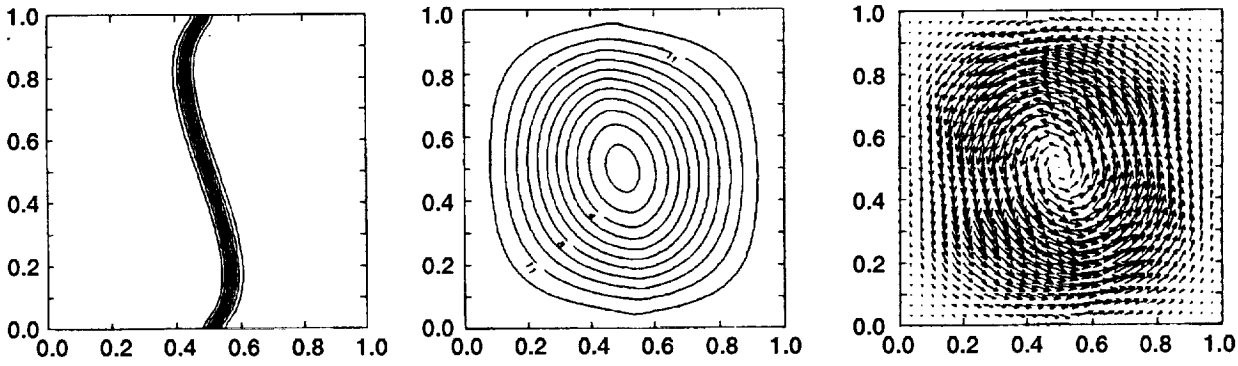

Figure 3A.—Destability of shear flow due to background rotational flow.

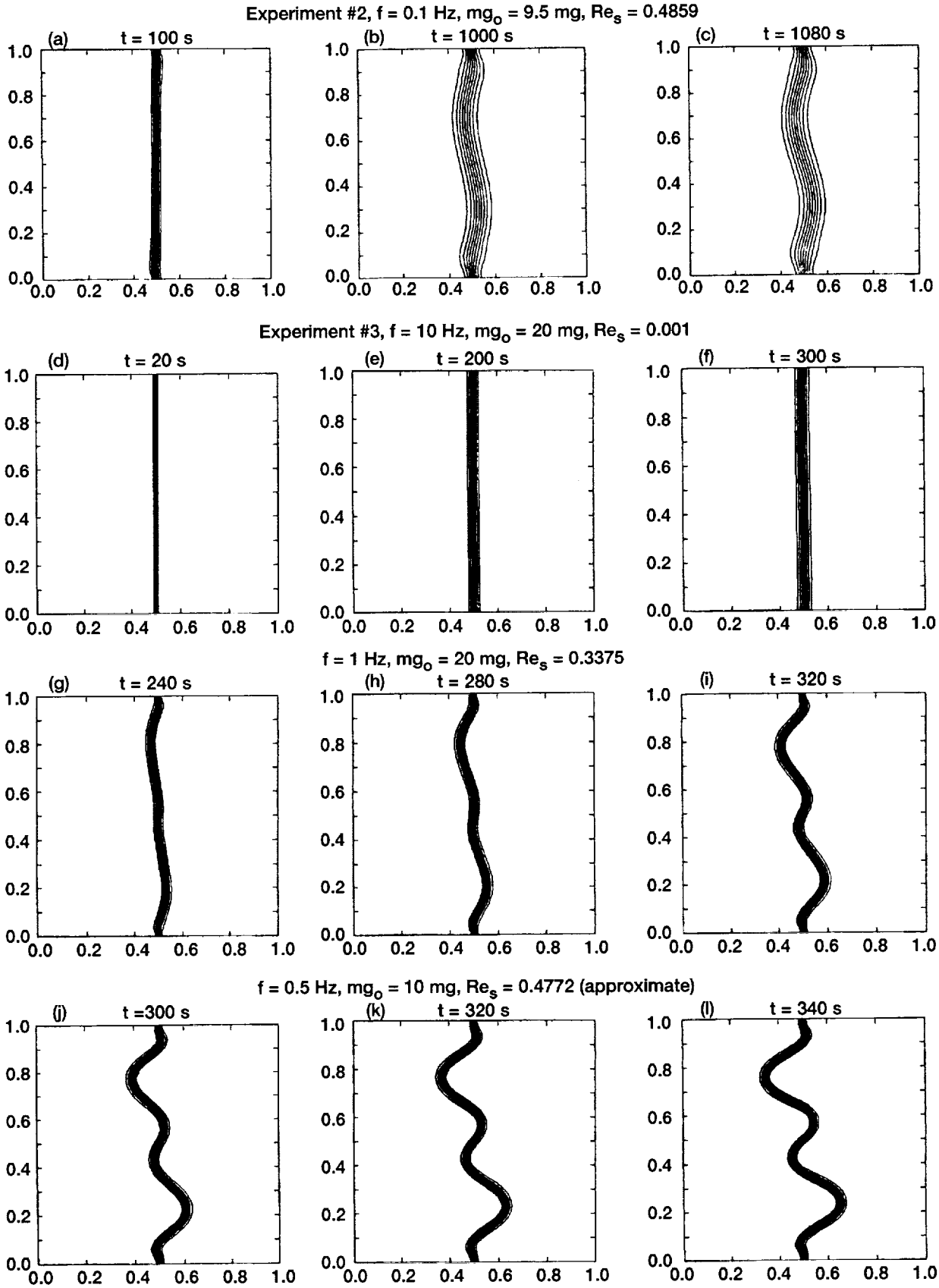

Figure 3B.—Evolution of the interface for solution starting from zero time, background g-level $ng_o = 10^{-6}\ g_o$.

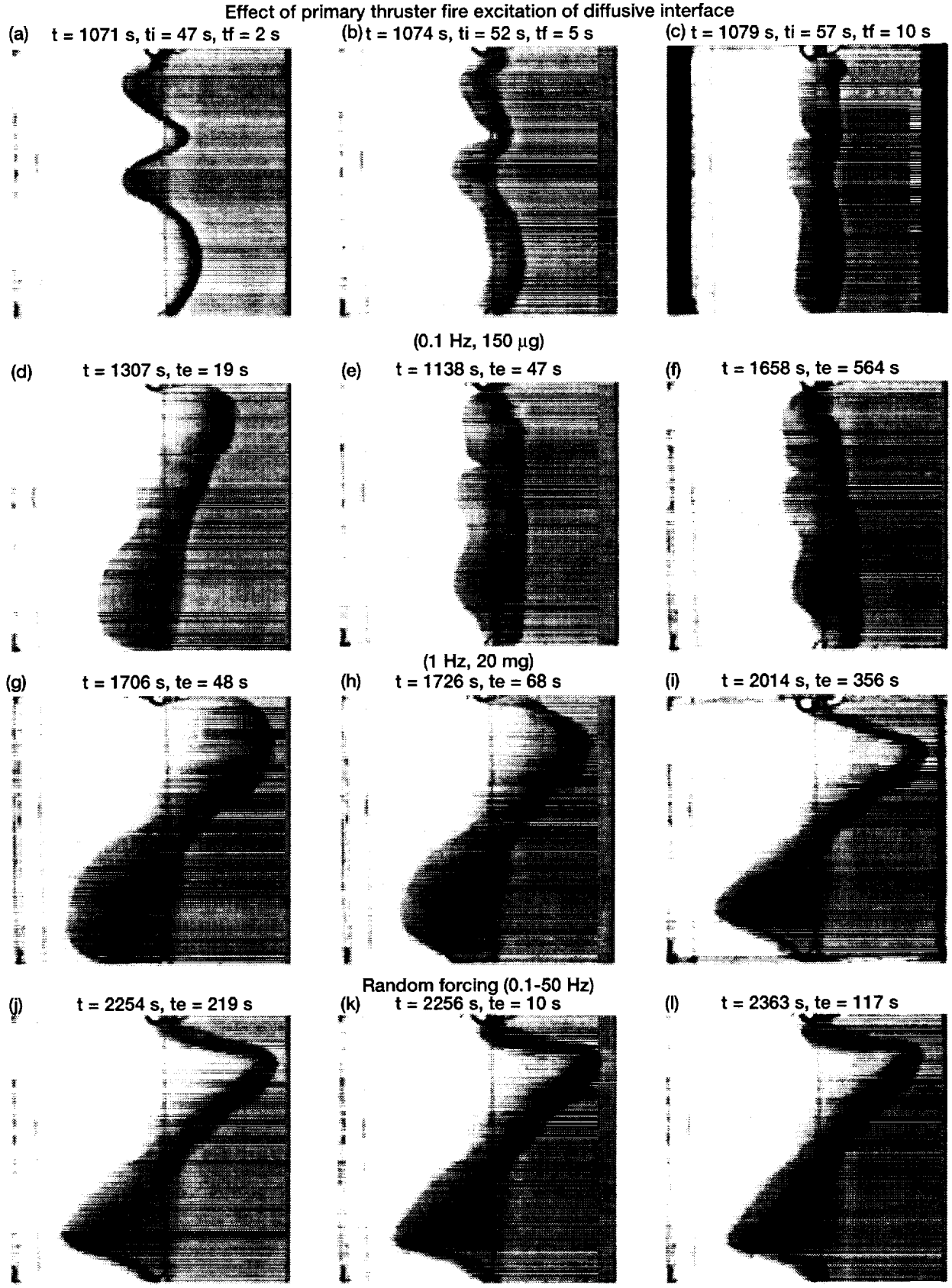

Figure 4.—Catastrophic bifurcation due to thruster fire and effects of sinusoidal and random forcing on interface, (t - time relative to shim removal, ti - isolation time, te - excitation time, tf - time relative to thruster fire).

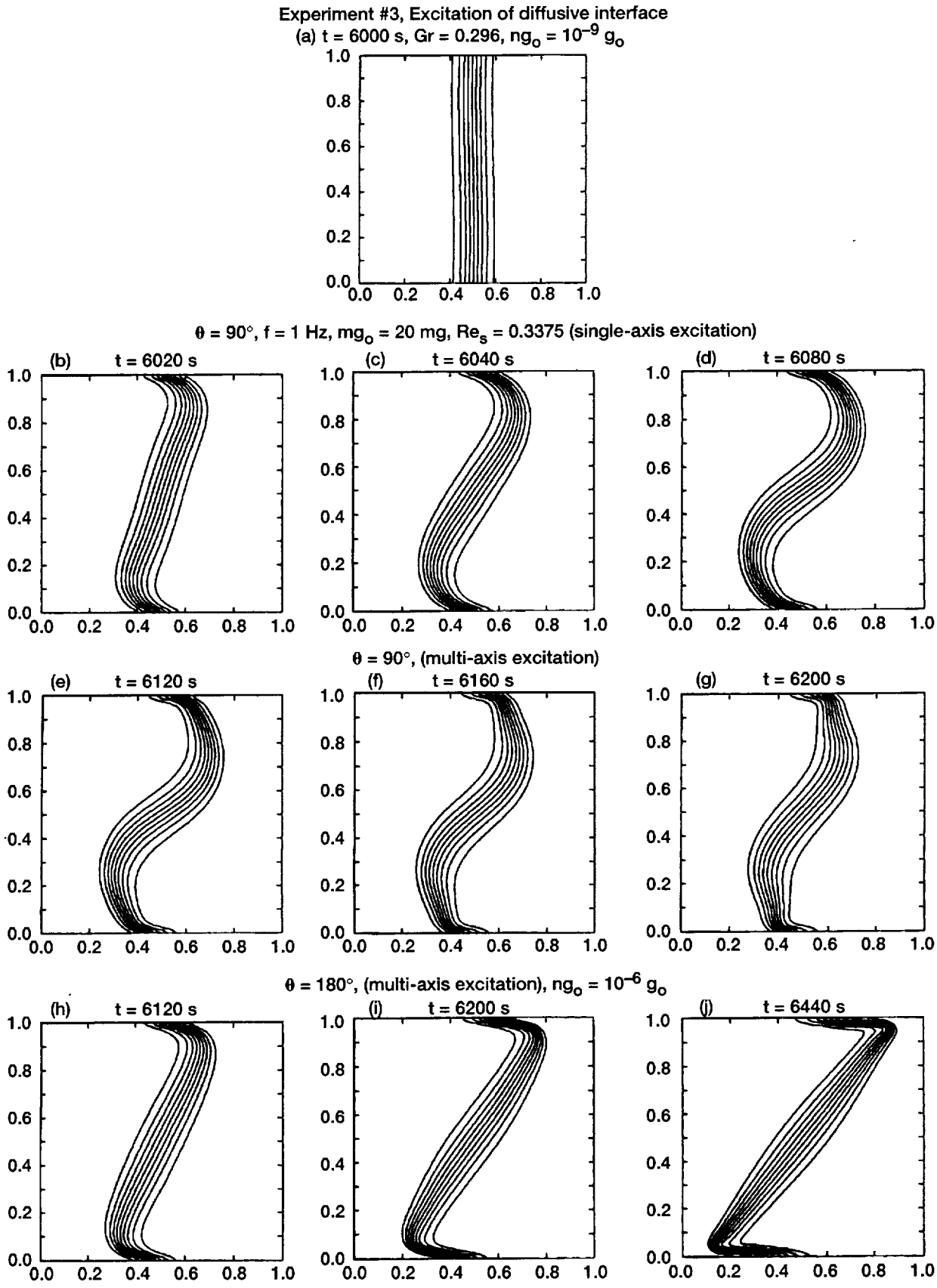

Figure 4A.—Single and multi-axis excitation of diffusive interface.

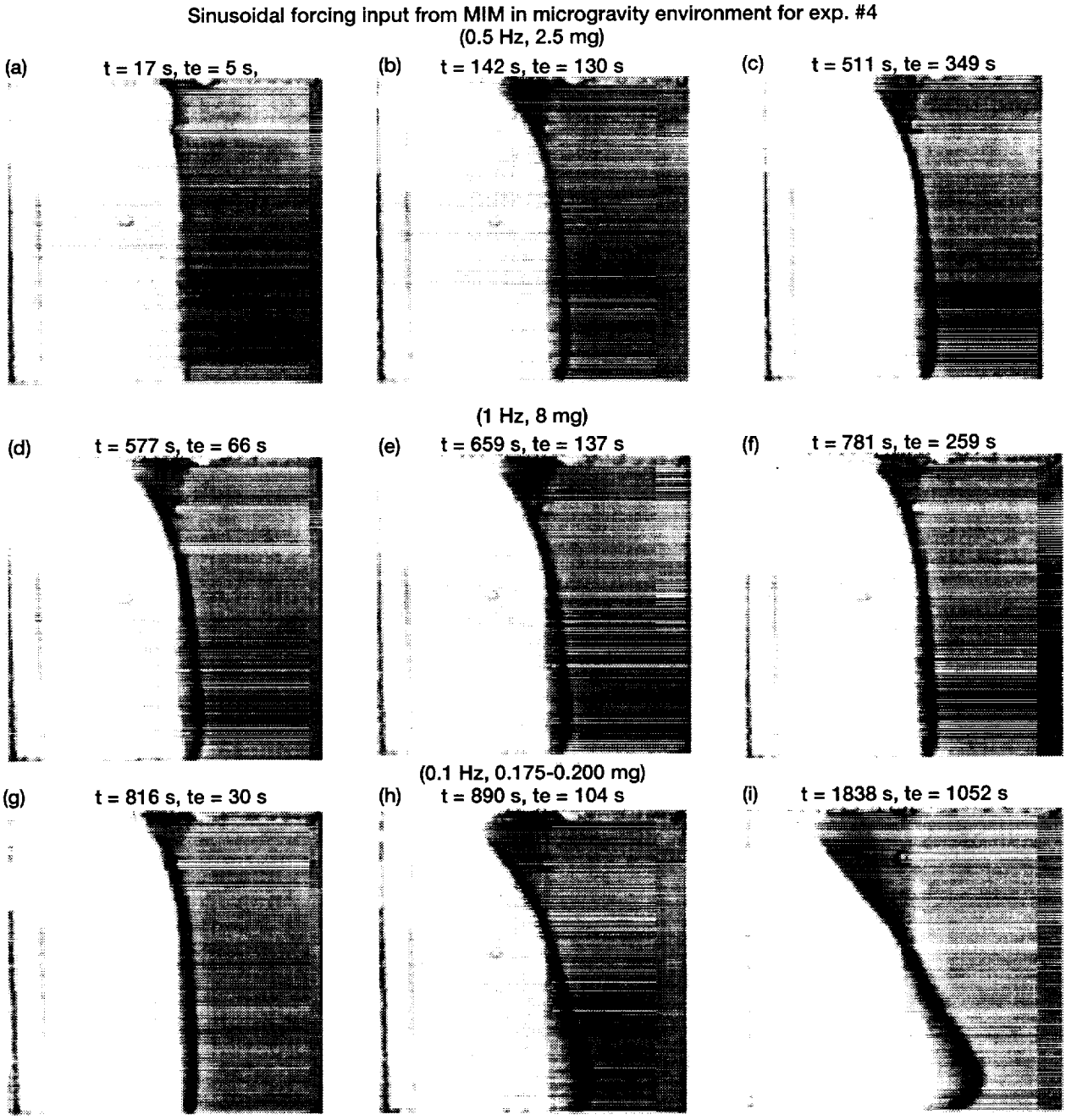

Figure 5.—Two mode bifurcation due to low amplitude sinusoidal forcing, (t - time relative to shim removal, ti - isolation time, te - excitation time, tf - time relative to thruster fire).

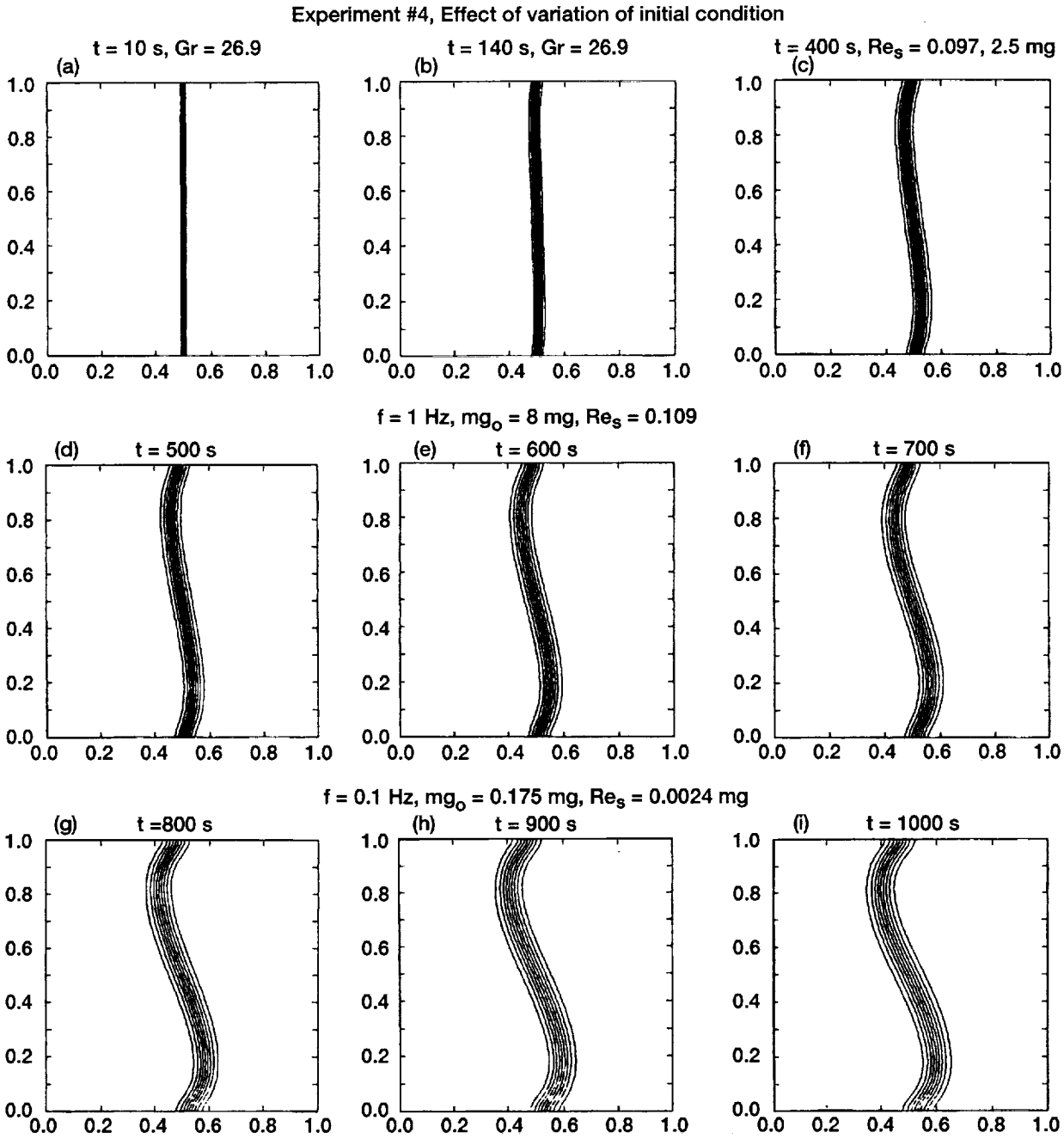

Figure 5A.—Symmetric two mode bifurcation, (g, h, i) solution starts from time zero, background g-level $ng_o = 10^{-6}\ g_o$.

REPORT DOCUMENTATION PAGE

Form Approved
OMB No. 0704-0188

1. AGENCY USE ONLY (*Leave blank*)	2. REPORT DATE	3. REPORT TYPE AND DATES COVERED
	March 2000	Technical Memorandum

4. TITLE AND SUBTITLE

Effects of G-Jitter on Interfacial Dynamics of Two Miscible Liquids: Application of MIM

5. FUNDING NUMBERS

WU-101-53-00-00

6. AUTHOR(S)

Walter M.B. Duval and Bjarni V. Tryggvason

7. PERFORMING ORGANIZATION NAME(S) AND ADDRESS(ES)

National Aeronautics and Space Administration
John H. Glenn Research Center at Lewis Field
Cleveland, Ohio 44135-3191

8. PERFORMING ORGANIZATION REPORT NUMBER

E-12073

9. SPONSORING/MONITORING AGENCY NAME(S) AND ADDRESS(ES)

National Aeronautics and Space Administration
Washington, DC 20546-0001

10. SPONSORING/MONITORING AGENCY REPORT NUMBER

NASA TM—2000-209789

11. SUPPLEMENTARY NOTES

Prepared for the 37th Aerospace Sciences Meeting and Exhibit sponsored by the American Institute of Aeronautics and Astronautics, Reno, Nevada, January 11-19, 1999. Walter M.B. Duval, NASA Glenn Research Center; and Bjarni V. Tryggvason, Canadian Space Agency, Saint-Hubert, Quebec, Canada J3y8y9. Responsible person, Walter M.B. Duval, organization code 6712, (216) 433-5023.

12a. DISTRIBUTION/AVAILABILITY STATEMENT

Unclassified - Unlimited
Subject Categories: 29 and 34 Distribution: Standard

This publication is available from the NASA Center for AeroSpace Information, (301) 621-0390.

12b. DISTRIBUTION CODE

13. ABSTRACT ***(Maximum 200 words)***

We designed an experiment to examine the effects of g-jitter on mixing of two miscible liquids using the Microgravity Vibration Isolation Mount (MIM). The global bifurcation of the interface was observed with the MIM operating alternatively to either transmit the g-jitter, isolate from the g-jitter or to provide controlled vibration levels with well defined amplitude and frequency content. With the MIM in isolation mode, the interface remains stationary indicating buoyancy induced convection is negligibly small such that mixing occurs via intrinsic mass diffusion without the masking effect of vibration driven convection. Analytical and computational results are in agreement with the experimental findings. Operation of the MIM in forced mode with conditions typical of g-jitter shows that vibration induced convective flows can excite instability mechanisms such as Kelvin-Helmholtz to generate large amplitude quasi-stationary waves oriented vertically for various cases with Stokes-Reynolds number in the range of 0.003 to 0.5. The two and four mode quasi-stationary waves are also predicted with a mathematical model. Though unplanned, the effect of a primary thruster firing was captured and shown to cause a catastrophic bifurcation, enhancing local mass transport. In light of the findings, experiments planned for the International Space Station should consider the potential effects of g-jitter.

14. SUBJECT TERMS

Miscible liquids; Wave structure; G-jitter; Phase angle, Microgravity

15. NUMBER OF PAGES

36

16. PRICE CODE

A03

17. SECURITY CLASSIFICATION OF REPORT	18. SECURITY CLASSIFICATION OF THIS PAGE	19. SECURITY CLASSIFICATION OF ABSTRACT	20. LIMITATION OF ABSTRACT
Unclassified	Unclassified	Unclassified	